Simulation of fluid-structure interaction in a microchannel using the lattice Boltzmann method and size-dependent beam element on a graphics processing unit

Vahid Esfahanian†, Esmaeil Dehdashti, and Amir Mehdi Dehrouye-Semnani

Department of Mechanical Engineering, University of Tehran, Tehran 515-14395, *Iran*

(Received 5 September 2013; revised manuscript received 13 January 2014; published online 20 June 2014)

Fluid-structure interaction (FSI) problems in microchannels play a prominent role in many engineering applications. The present study is an effort toward the simulation of flow in microchannel considering FSI. The bottom boundary of the microchannel is simulated by size-dependent beam elements for the finite element method (FEM) based on a modified couple stress theory. The lattice Boltzmann method (LBM) using the D2Q13 LB model is coupled to the FEM in order to solve the fluid part of the FSI problem. Because of the fact that the LBM generally needs only nearest neighbor information, the algorithm is an ideal candidate for parallel computing. The simulations are carried out on graphics processing units (GPUs) using computed unified device architecture (CUDA). In the present study, the governing equations are non-dimensionalized and the set of dimensionless groups is exhibited to show their effects on micro-beam displacement. The numerical results show that the displacements of the micro-beam predicted by the size-dependent beam element are smaller than those by the classical beam element.

Keywords: fluid-structure interaction, graphics processing unit, lattice Boltzmann method, size-dependent beam element

PACS: 47.61.−k, 07.10.Cm, 47.61.Fg, 81.40.−z **DOI:** 10.1088/1674-1056/23/8/084702

1. Introduction

Due to the recent rapid development of micro flow devices applied in micro-total-analysis-systems (m-TAS) and micro-electro-mechanical systems (MEMS), modeling and simulation methods for flows in such micro-geometries have been of great interest in the society of computational physics.[1] The design of stirrers, extruders, and injection systems in process engineering or artificial heart valves and blood vessels in medicine requires the consideration of the bidirectional interaction between fluid and structure as well.

In general, two approaches to solve FSI problems exist. The monolithic approach[2] discretizes the two separate domains with a similar discretization scheme and solves the resulting, coupled system of equations within one solver. The compatibility conditions at the interface are treated inherently within this system of equations. By contrast, the partitioned approach[3] uses separate solvers for the fluid and the structural system. Strong coupling methods[4] as well as loose coupling methods[5] exist. In the partitioned solution, the solvers need to communicate the physical properties of their mutual boundary to fulfill the interface conditions. Each domain may utilize any type of discretization considered efficient for its field.

Several numerical techniques have also been developed for FSI problems using the macroscopic continuity and momentum equations for flow field. Some of them used FEM for both fluid and structure analyses,[6,7] and some others used coupled FEM and the boundary element method.[8,9] Most of those studies considered potential flow for FSI. Viscous flow was considered in blood flow using FEM.[10,11]

In the micro-indentation experiments in 1995, Ma and Clarke[12] observed that the measured indentation hardness of silver single crystal increases by a factor of more than two as the penetration depth of the indenter decreases from 2.0 μm to 0.1 μm. In the micro-bending test of thin nickel beams in 1998, Stolken and Evans[13] observed that the plastic work hardening shows a great increase as the beam thickness decreases from 50 μm to 12.5 μm. Currently, the size dependences are observed in some polymers deformed elastically. For example, in the micro-bending testing of epoxy polymeric beams in 2002, Lam *et al.*[14] observed that the bending rigidity increases about 2.4 times as the beam thickness reduces from 115 μm to 20 μm. In the micro-bending testing of polypropylene micro-cantilevers in 2005, McFarland *et al.*[15] observed that the measured stiffness values are seen to be at least four times larger than the classical beam theory stiffness predictions and the deformation is also in the range of linear elastic cases.

The experimental results show that the size dependence is intrinsic to certain materials with non-homogeneous microstructure. Therefore, accurate characterization of these dynamic mechanical properties in the micron scale is urgent and vital for the reliable and optimal design of many devices.[16]

Beam models based on classical elasticity are not capable of describing such size effects due to the lack of a material length scale parameter. This motivated the development of

†Corresponding author. E-mail: evahid@ut.ac.ir

© 2014 Chinese Physical Society and IOP Publishing Ltd

beam models using higher-order (non-local) continuum theories that contain additional material constants. In view of the difficulties in determining microstructure-dependent length scale parameters[17] and the approximate nature of beam theories, non-classical beam models involving only one material length scale parameter are desirable. One such model has recently been developed for the Bernoulli–Euler beam by Park and Gao[18] using a modified coupled stress theory proposed by Yang *et al.*,[19] which contains only one material length scale parameter. The characteristics of microtubes conveying fluid considering the modified couple stress theory were studied by Wang[20] and Xia and Wang.[21] The flexural vibrations of microscale pipes conveying fluid were also studied by Wang.[22] The modified coupled stress theory was employed to develop a size-dependent beam element able to predict the size-dependency observed in microbeams by Kahrobaiyan *et al.*[23]

The Navier–Stokes (macroscopic momentum) equations are no longer applicable to micro-flows (levels of moderately high Knudsen number) and the flow physics in such flows is described by the Boltzmann equation (BE) of the gas kinetic theory.[24] Moreover, an advantage of the LBM compared to conventional computational fluid dynamics (CFD) solvers is the local availability of the stress tensor. For example, problems such as multiphase flows,[25,26] turbulent flow,[27,28] and thermal flow[29–31] could be handled effectively using the LBM. The first LB algorithm for an interaction problem between a fluid and rigid obstacles has been developed by Ladd[32,33] for the simulation of particulate suspensions. An application of the LBM to FSI was the case with flow around rigid structures as appeared in artificial heart-valve geometries.[34] Moreover, coupling of LBM to FEM for FSI application was undertaken in a staggered manner for D2Q9 LB model.[35] The D2Q9 LB model can only capture the basic feature at sufficiently small Knudsen numbers. The higher-order LB method improves the accuracy in micro-flows (finite Knudsen number), as has already been compared with the standard LB method. The transient bidirectional FSI problem was investigated with geometrically nonlinear structural deflections.[36] However, to the best knowledge of the authors, there have been few efforts to couple the LBM to the FEM to solve the fluid and flexible structure interaction problems in microscale considering the microstructure-dependent size effects in micro-beams.

Because of the fact that the LBM generally needs only nearest neighbor information, the algorithm is an ideal candidate for parallel computing. The first application of GPU on LBM modeling used a NVIDIA Geforce4 Ti4600 card with 128-MB memory.[37] Later, however, special codes needed to be used for different types of hardware. Then, the CUDA was launched by NVIDIA in 2007 for simplifying the computing code writing for GPU massively parallel programming. For example, the computational efficiency has been improved by using an NVIDIA GTX 280 CUDA-enabled graphics card on 2D LBM codes.[38]

In the present study, two-dimensional flow is solved in a microchannel, as shown in Fig. 1. To simulate a microchannel, the D2Q13 LB model is applied using the staggered manner to couple the LBM and the FEM to solve the FSI problem. The top boundary is assumed to be rigid while the bottom boundary is considered to be flexible. The flexible boundary is modeled as a Bernoulli–Euler beam clamped at both end points. The modified couple stress theory is applied to solve the dynamic problem of the Bernoulli–Euler beam. The simulations are carried out on GPU using CUDA. In the present study, the governing equations are non-dimensionalized and the set of dimensionless groups is presented to show their effects on micro-beam displacement. The numerical results show that the displacements of the micro-beam predicted by the size-dependent beam element are smaller than those by the classical beam element.

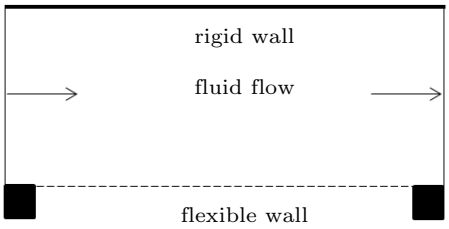


Fig. 1. Flow between rigid and flexible walls in a microchannel.

2. Lattice Boltzmann method

The LBM was originated from lattice gas (LG) automata,[39] which are discrete particle kinetics based on discrete time and lattice spaces. The LB equation is expressed as:

$$f_i(\boldsymbol{x}+\boldsymbol{e}_i\Delta t, t+\Delta t) - f_i(\boldsymbol{x},t) = \Omega_i(f(\boldsymbol{x},t)), \tag{1}$$

where $f_i(\boldsymbol{x},t)$ denotes the probability of finding a particle at lattice site $\boldsymbol{x}$ and time t, which moves with the local particle velocity $\boldsymbol{e}_i$. Furthermore, Δt is the time increments, and Ω_i is the collision operator for the rate of change of f_i resulting from collision, and it depends only on the local value of $f_i(\boldsymbol{x},t)$.

In Eq. (1), the local particle velocity $\boldsymbol{e}_i$ is discrete in the given lattice. For a D2Q13 lattice model, as shown in Fig. 2, the discrete velocities for the thirteen possible directions are:

$$\begin{aligned}
e_0 &= 0,\\
e_i &= \left[\cos\left(\frac{((i-1)\pi)}{2}\right), \sin\left(\frac{((i-1)\pi)}{2}\right)\right]c, \quad i = 1\text{–}4,\\
e_i &= \left[\cos\left(\frac{((i-5)\pi)}{2}+\frac{\pi}{4}\right), \sin\left(\frac{((i-5)\pi)}{2}+\frac{\pi}{4}\right)\right]\sqrt{2}c, \quad i = 5\text{–}8,\\
e_i &= \left[\cos\left(\frac{((i-1)\pi)}{2}+\frac{\pi}{4}\right), \sin\left(\frac{((i-1)\pi)}{2}+\frac{\pi}{4}\right)\right]2c, \quad i = 9\text{–}12,
\end{aligned}$$

where $c = \Delta x/\Delta t$ and Δx is the lattice spacing step. For the BGK model,[40] the collision operator is expressed as:

$$\Omega_i = -\frac{f_i(\boldsymbol{x},t) - f_i^{(\mathrm{eq})}(\boldsymbol{x},t)}{\tau},$$

where τ is the relaxation time and $f_i^{(\mathrm{eq})}$ denotes the local equilibrium distribution. This local equilibrium is derived from the Maxwell–Boltzmann equilibrium distribution. The equilibrium distribution is defined as:

$$f_i^{(\mathrm{eq})} = \rho w_i\Big[1 + \frac{e_{ik}u_k}{c_\mathrm{s}^2} + \frac{(e_{ik}u_k)^2}{2c_\mathrm{s}^2} - \frac{u_k u_k}{2c_\mathrm{s}^2} + \frac{(e_{ik}u_k)^3}{2c_\mathrm{s}^6} - \frac{3(e_{ik}u_k)(u_k u_k)}{2c_\mathrm{s}^4}\Big], \tag{2}$$

in which ρ is the fluid density, u is the fluid velocity, and $c_\mathrm{s} = c/\sqrt{2}$ is the lattice speed of sound. Where the weight coefficients in Eq. (2) are as:

$$\begin{aligned} w_0 &= \frac{3}{8}, \\ w_i &= \frac{1}{12}, \qquad i = 1\text{–}4, \\ w_i &= \frac{1}{16}, \qquad i = 5\text{–}8, \\ w_i &= \frac{1}{96}, \qquad i = 9\text{–}12. \end{aligned}$$

The fluid density ρ and momentum density $\rho\boldsymbol{u}$ are expressed as:

$$\rho = \sum_{i=0}^{12} f_i,$$
$$\rho\boldsymbol{u} = \sum_{i=0}^{12} \boldsymbol{e}_i f_i.$$

Furthermore, it can be shown that the pressure fluid p and the kinematic viscosity ν derived from the Boltzmann BGK equation through the Chapman–Enskog expansion is:

$$p = c_\mathrm{s}^2\rho,$$
$$\nu = \Delta t c_\mathrm{s}^2(\tau - 0.5).$$

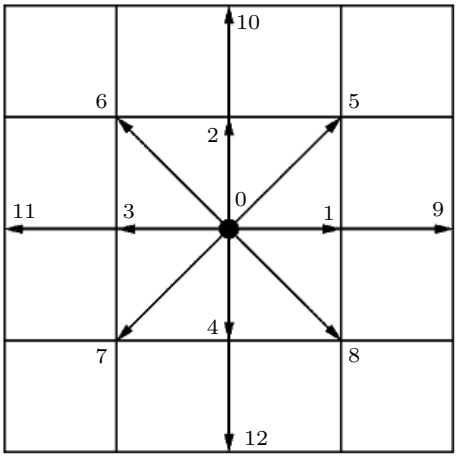


Fig. 2. LB model with 13 discrete velocity vectors.

In equilibrium, the conservation of mass and momentum is satisfied at each lattice:

$$\sum_{i=0}^{12} \Omega_i = 0,$$
$$\sum_{i=0}^{12} \Omega_i \boldsymbol{e}_i = 0.$$

3. Finite element method

The flexible boundary is modeled as a micro-beam clamped at both end points. The cross section of the micro-beam is rectangular. The total length of the microscale beam is L_x, the cross-section height and width of that beam are h, l_y, respectively. The Cartesian axes for beam analysis are established, as shown in Fig. 3. The dynamic governing equation of the beam in terms of $w(\boldsymbol{x},t)$ is given by

$$(EI + GAl^2)\frac{\partial^4 w}{\partial x^4} + \rho A\frac{\partial^2 w}{\partial t^2} = q(\boldsymbol{x},t), \tag{3}$$

where $w(\boldsymbol{x},t)$ is the z component of the displacement vector, I is the usual second moment of cross-sectional area, and A is the cross-sectional area of the beam, E, G are the Young modulus and the shear modulus, respectively. q is transverse loading and ρ is the density of the beam material. l is a material length scale parameter.

The boundary conditions for solving Eq. (3) are considered as:

$$\begin{cases} \dfrac{\partial w(\boldsymbol{x},t)}{\partial x} = 0, & \text{at} \quad x = 0, L_x, \\ w(\boldsymbol{x},t) = 0, & \text{at} \quad x = 0, L_x. \end{cases}$$

It can be seen from Eq. (3) that the equilibrium relations of the beams are related to two parts: one associated with ρA and EI as in the classical beam model and the other associated with GAl^2. Also, it should be emphasized that the current beam model based on the modified couple stress theory contains only one additional material constant besides the two classical material parameters. Nevertheless, the presence of l enables the incorporation of the material size features in the new model and renders it possible to explain the size effect.[16] Furthermore, when the size effect is suppressed by letting $l = 0$, the new model will reduce to the classical beam model.

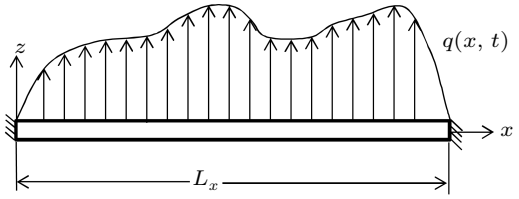


Fig. 3. Schematic diagram of Cartesian coordinate system for the Bernoulli–Euler beam.

When the microstructural effect is considered, substituting $(EI)^\star$ instead of $EI + GAl^2$, equation (3) can be written

as

$$(EI)^{\star}\frac{\partial^4 w}{\partial x^4}+\rho A\frac{\partial^2 w}{\partial t^2}=q(\boldsymbol{x},t), \tag{4}$$

which is identical to the governing equation derived in a macroscale beam with equivalent flexural rigidity $(EI)^{\star}$.

4. Coupling of LBM and FEM

One of the boundary conditions at the fluid-structure interface is given as:

$$v=\frac{\partial w}{\partial t},$$

where w is the z component of the structural displacement vector at the fluid-structure boundary and this equation states the continuity of velocity at the boundary. Furthermore, the continuity of traction at the fluid-structure boundary is expressed as

$$\sigma^{\mathrm{f}}_{kl}n_l=\sigma^{\mathrm{s}}_{kl}n_l.$$

An advantage of the LBM compared to conventional CFD solvers is the local availability of the stress tensor.[35] The stress tensor σ^{f}_{kl} with scalar pressure is:

$$\sigma^{\mathrm{f}}_{kl}=-p\delta_{kl}+S_{kl}. \tag{5}$$

S_{kl} is computed from the non-equilibrium part of the distributions and δ is the Kronecker-delta.[41]

$$S_{kl}=\left(1-\frac{1}{2\tau}\right)\sum_{i=0}^{12}f_i^{(\mathrm{neq})}\left(e_{ik}e_{il}-\frac{1}{2}e_ie_i\delta_{kl}\right).$$

Coupling of the LBM to the FEM for FSI application is undertaken in a staggered manner. In other words, the LBM is applied to the fluid domain using the velocity boundary conditions obtained from the FEM at the fluid-structure interface. Then, the fluid traction is computed from the LBM at the fluid-structure boundary. The traction is applied to the structural finite element analysis. This solution cycle is continued until the solutions for the fluid and structure become compatible at the interface boundaries.

A procedure to apply the fluid-structure interface velocity boundary condition to the LBM is described below. First of all, the boundary condition scheme is applied to the fluid-structure boundary lattice points of the LBM. Then, the local particle distribution f_i is further modified as follows to maintain the velocity continuity at the fluid-structure boundary. Let $\dot{w}_x$ and $\dot{w}_y$ be the structural velocity components along the x and y axes at the fluid-structure interface. The particle distribution is revised as follows:

$$f_1=f_1+\frac{\dot{w}_x}{2},\quad f_2=f_2+\frac{\dot{w}_y}{2},\quad f_3=f_3-\frac{\dot{w}_x}{2},\quad f_4=f_4-\frac{\dot{w}_y}{2},$$
$$f_5=f_5+\frac{2\dot{w}_x}{3}+\frac{2\dot{w}_y}{3},\quad f_6=f_6-\frac{2\dot{w}_x}{3}+\frac{2\dot{w}_y}{3},$$
$$f_7=f_7-\frac{2\dot{w}_x}{3}-\frac{2\dot{w}_y}{3},\quad f_8=f_8+\frac{2\dot{w}_x}{3}-\frac{2\dot{w}_y}{3},$$
$$f_9=f_9+4\dot{w}_x,\quad f_{10}=f_{10}+4\dot{w}_y,\quad f_{11}=f_{11}-4\dot{w}_x,$$
$$f_{12}=f_{12}-4\dot{w}_y.$$

When the traction was computed from the LBM using Eq. (5), then the finite element analysis by using Eq. (4) is conducted using the following equation:

$$[M]\{\ddot{w}\}+[K]\{w\}=\{F\}+\{P\},$$

where $[M]$ and $[K]$ which is obtained for the micro-finite-element model by Kahrobaiyan *et al.*,[23] are the finite element mass and stiffness matrices, respectively. Furthermore, $\{F\}$ is the external force vector and $\{P\}$ is the force vector resulting from the FSI, as expressed below

$$\{P\}=\sum\int_{\Gamma_{\mathrm{int}}}[N]^{\mathrm{T}}\{r\}\,\mathrm{d}\Gamma.$$

Here, $[N]$ is the matrix composed of finite element shape functions over the interface element boundary Γ_{int}, and $\{r\}$ is the traction vector. The summation is over the total number of finite element boundaries at the fluid-structure interface.

5. Numerical results

In the present study, two-dimensional flow in a microchannel is solved. The D2Q13 LB model using a technique to couple the LBM and the FEM is applied to solve FSI problems.[35] The top boundary is assumed to be rigid while the bottom boundary is considered to be flexible. The flexible boundary is modeled as a Bernoulli–Euler beam clamped at both end points. The non-equilibrium extrapolation boundary condition is used for the flow field.[42]

Writing non-dimensional forms of the governing equations can yield insight into the underlying physical phenomena, and indicate which forces are dominant. If two dynamically similar but different property flows do exist, the equations would only yield the same mathematical results if the two flows had the same values for the dimensionless groups. In the present study, the governing equations are non-dimensionalized and the set of dimensionless groups, as shown in Table 1, is exhibited to show their effects on microbeam displacement. Where p, u_0, and ν are fluid pressure, inlet flow velocity, and viscosity of the fluid, respectively. ρ_{f}, ρ_{s} are the fluid and solid density, respectively and l_z is the height of the microchannel.

Table 1. Definition of dimensionless groups.

Dimensionless group	Formula	Name
Π_1	$(L_x)/h$	length-to-height ratio of the beam
Π_2	h/l	material length-to-height ratio of the beam
Π_3	p/E	pressure-to-Young's modulus ratio
Π_4	$(u_0 l_z)/\nu$	Reynolds number (Re)
Π_5	$\sqrt{\rho_{\mathrm{s}}/E}\,u_0$	elastic number
Π_6	$\rho_{\mathrm{f}}/\rho_{\mathrm{s}}$	density ratio

5.1. Grid-independent validation

A grid analysis was performed using different grid sizes. The size of the grids used in the analysis were 100×50, 200×100 , 300×150. As shown in Fig. 4, different grids have no effect in the displacement of the center of a micro-beam. The final value of displacement in each case is the same. Considering the results provided by this analysis, it is determined that using a coarse grid in this study would provide reasonable accuracy and avoid high computational cost.

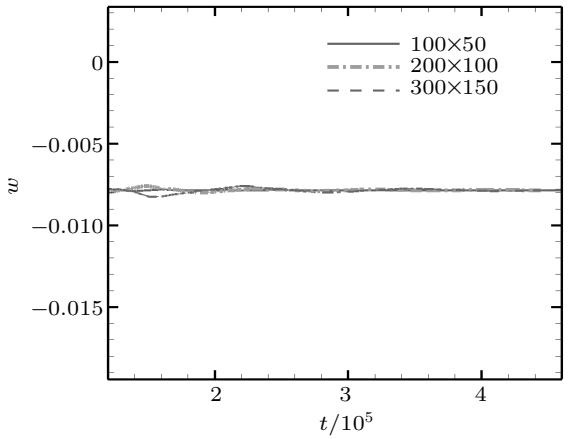


Fig. 4. Effect of the grid on the displacement at the center of the micro-beam with classical theory and $Re = 80$, $\Pi_3 = 5 \times 10^{-7}$, $\Pi_5 = 0.04$, $\Pi_6 = 0.1$.

5.2. Results and discussion

Effects of Π_2 to Π_6 are studied on the displacement of a micro-beam as follows. As the fluid flows, the flexible beam vibrates up and down. The time history of the vibrational motion of the flexible beam at the center is shown in the following figures. In all plots, displacements are non-dimensionalized with respect to the lattice grid size while time is normalized in terms of the time increment. Figure 5 indicates that an increase of Π_2 increases the displacement of the micro-beam and the results converge to classical model results. Because an increase of Π_2 means a decrease of l, the model will reduce to the classical beam model. By the way, the bending stiffness, considering the microstructural effect, is equal to $EI + GAl^2$ instead of EI. So, the bending stiffness considering the microstructural effect increased and the displacement of the micro-beam decreased. The vibrations are invisible in Fig. 5, with magnifying the vibrations are plotted in Fig. 6.

The increase of Π_3 means the flow pressure which forcing to the boundary increases or the micro-beam has less Young's modulus, so that both of them make more displacement, as can be seen in Fig. 7. As shown in Fig. 8, when Π_5 increases, the vibrational amplitude increases, which means for a micro-beam with known properties, when the flow velocity increases, the vibrational amplitude of the micro-beam increases.

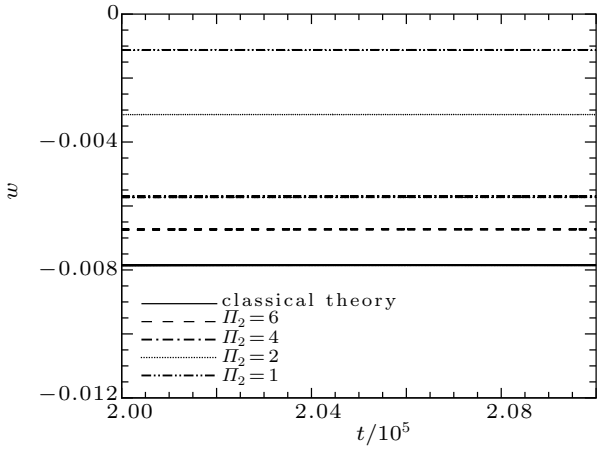


Fig. 5. Time history plot of the displacement at the center of the micro-beam with $Re = 50$, $\Pi_3 = 5 \times 10^{-7}$, $\Pi_5 = 0.04$, $\Pi_6 = 0.1$, and different Π_2.

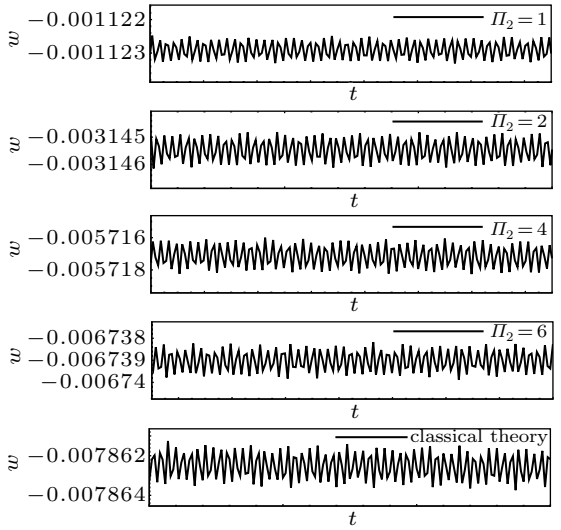


Fig. 6. Magnified displacement at the center of the micro-beam with $Re = 50$, $\Pi_3 = 5 \times 10^{-7}$, $\Pi_5 = 0.04$, $\Pi_6 = 0.1$, and different Π_2.

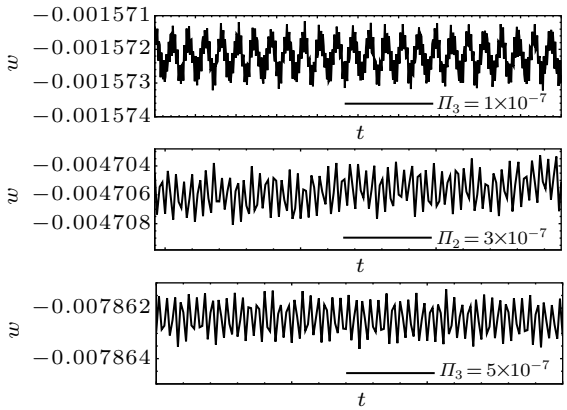


Fig. 7. The displacement at the center of the micro-beam with $Re = 50$, $\Pi_2 = 0$, $\Pi_5 = 0.04$, $\Pi_6 = 0.1$, and different Π_3.

The displacement for different Π_6 is shown in Fig. 9, which indicates vibrational amplitude decreases, when Π_6 increases. The Reynolds number, which is an important property of flow that determines whether flow is formed in a laminar or

turbulent way, is now considered. Figure 10 shows the displacement in different Reynolds numbers.

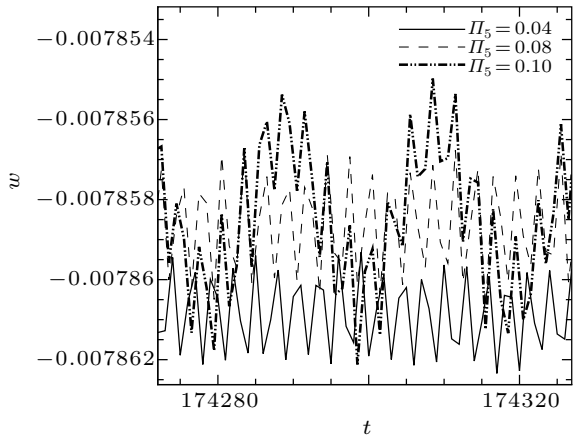


Fig. 8. The displacement at the center of the micro-beam with $Re = 50$, $\Pi_2 = 0$, $\Pi_3 = 5 \times 10^{-7}$, $\Pi_6 = 0.1$, and different Π_5.

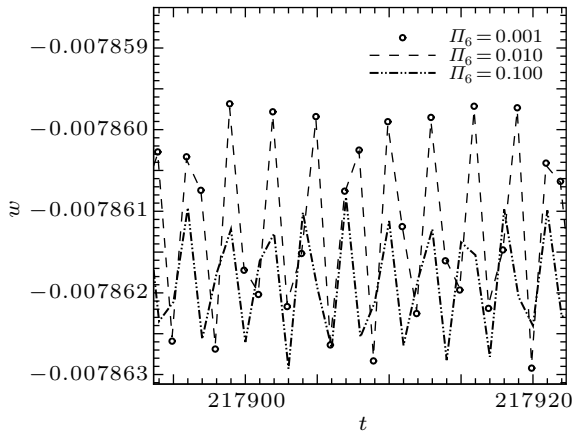


Fig. 9. The displacement at the center of the micro-beam with $Re = 50$, $\Pi_2 = 0$, $\Pi_3 = 5 \times 10^{-7}$, $\Pi_5 = 0.04$, and different Π_6.

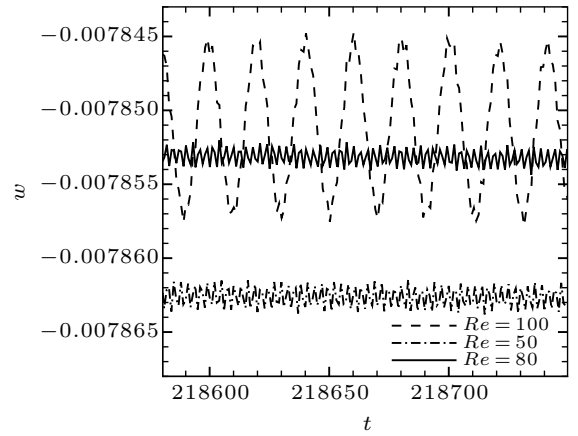


Fig. 10. The displacement at the center of the micro-beam with $\Pi_2 = 0$, $\Pi_3 = 5 \times 10^{-7}$, $\Pi_5 = 0.04$, $\Pi_6 = 0.1$, and different Re.

At a low Reynolds number, the laminar flow is steady. But if the Reynolds number is increased more, the interaction between flow and structure can cause an unsteady laminar flow, as shown in Fig. 11, for the Reynolds number equal to 150 using classical theory. The displacement along the Bernoulli–Euler beam at different time steps is also shown in Fig. 12. Moreover, when Π_2 increases, the bending stiffness of the micro-beam decreases. Therefore, using less Π_2 fluid flow, which was unsteady (see Fig. 11), can be steady, as shown in Fig. 13, using Π_2 equal to 1.

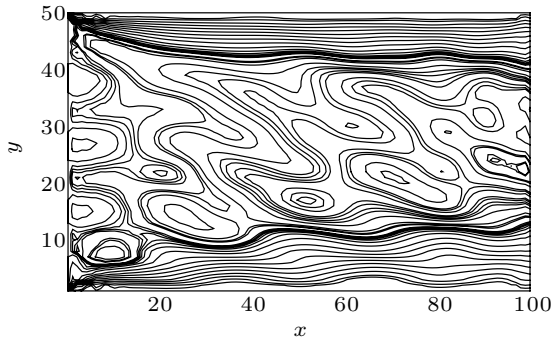


Fig. 11. The horizontal velocity contours of the unsteady laminar flow with classical theory and $Re = 150$, $\Pi_3 = 5 \times 10^{-7}$, $\Pi_5 = 0.04$, and $\Pi_6 = 0.1$.

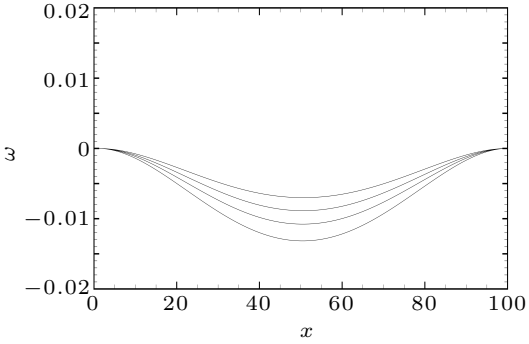


Fig. 12. The displacement along the Bernoulli–Euler beam at different time steps with classical theory and $Re = 150$, $\Pi_3 = 5 \times 10^{-7}$, $\Pi_5 = 0.04$, and $\Pi_6 = 0.1$.

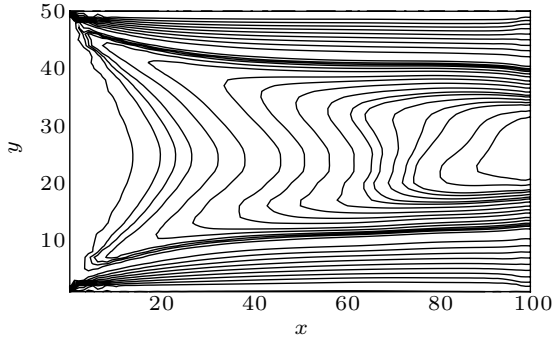


Fig. 13. The horizontal velocity contours of the steady laminar flow with $Re = 150$, $\Pi_2 = 1$, $\Pi_3 = 5 \times 10^{-7}$, $\Pi_5 = 0.04$, and $\Pi_6 = 0.1$.

6. GPU implementation

Different from the traditional central processing unit (CPU), a GPU has many arithmetic logical units (ALU), or threads, and fits massive parallel computations because the same program is executed on many data elements in parallel by using a significant amount of threads. This programmable GPU parallel technique has attracted much atten-

tion recently. In the CUDA program, the distribution functions are rewritten as thirteen 1D arrays on the system memory, $f_0[L], f_1[L], \ldots, f_{12}[L]$, where L is an index that varies from 0 to $[(GX+1)\times(GY+1)-1]$, with the general term as $(GX+1)\times y+x$, where x and y are integers that represent a node point in the lattice (i.e., $0 \le x \le GX, 0 \le y \le GY$).

Performance tests were made with an Intel Core 2 Due E7400 2.8 GHz. The GPU tests were made on a machine running on a Geforce GTX 480. Numerical investigations with different domain meshes are carried out for determining the parallel efficiency, as shown in Table 2. It must be noted that global memory is used, which makes less speed up than register or shared memories.

Table 2. Parallel performance.

Grid	100×50	200×100	300×150	400×200
Speedup	9.6	13.3	19.7	26.9

7. Conclusion

A coupling is used for the FSI application using the LBM for the fluid domain and the FEM for the structural domain. The higher-order LB method improves the accuracy in microflows (finite Knudsen number), as has already been compared with the standard LB method. The D2Q13 LB model is applied using the staggered manner to couple the LBM and the FEM to solve the microscale FSI problem. A size-dependent beam element for the Bernoulli–Euler beam is considered, which employs a modified coupled stress theory.[23] In modified coupled stress theory, one material length scale parameter is included to capture the size effect, unlike the classical Bernoulli–Euler beam theory.

In this paper, a lattice Boltzmann/FEM parallel GPU implementation is presented for the FSI problems with low Reynolds and small displacement fields in two dimensions. It was observed to have a great benefit in computational time when using the GPU implementation of the method. As mentioned before, global memory is used in the present study, but more speed up can be achieved by using register or shared memory in future works.

The numerical results show that the displacements of the micro-beam predicted by the size-dependent beam element are smaller than those by the classical beam element. Moreover, it is found that when the Reynolds number increases considering the classical element, the flow will be unsteady, but considering the non-classical element with enough small Π_2, the flow could be steady. Because the micro-beam considering a size-dependent beam element based on the modified coupled stress theory will be stiffer than a beam considering classical theory. The present work can be considered as a basic work for further study to build on. The microchannel can be simulated in the three-dimensional case by applying the three-dimensional LB model for the fluid domain and the plate element for the bottom boundary. Moreover, the LBM is useful to solve multiphase problems, hence the present study can be extended to simulate multiphase flows inside or outside flexible structures.

Acknowledgments

The authors would like to thank Vehicle, Fuel and Environment Research Institute (VFERI) of University of Tehran.

References

[1] Karniadakis G, Beskok A and Aluru N R 2005 *Microflows and Nanoflows: Fundamentals and Simulation* (New York: Springer)
[2] Walhorn E, Kölke A, Hübner B and Dinkler D 2005 *Comput. Struct.* **83** 2100
[3] LeTallec P and Mouro J 2001 *Comput. Method Appl. Mech. Eng.* **190** 3039
[4] Küttler U and Wall W 2009 *J. Appl. Mech.* **2** 76
[5] Löhner R, Cebral J R, Camelli F F, Baum J D, Mestreau E L and Soto O A 2007 *Arch. Comput. Method Eng.* **14** 279
[6] Bathe K J, Nitikipaiboon C and Wang X 1995 *Comput. Struct.* **56** 225
[7] Kwon Y W and McDermott P M 2001 *J. Pres. Ves. Technol.* **123** 480
[8] Everstine G C and Henderson F M 1990 *J. Acoust. Soc. Am.* **87** 1938
[9] Giordano J A and Koopmann G H 1995 *J. Acoust. Soc. Am.* **98** 363
[10] Dubini G, Pietrabissa R and Montevecchi F M 1995 *Med. Eng. Phys.* **17** 609
[11] Tienfuan K, Lee L L and Wellford L C 1997 *J. Fluids Eng. Trans. ASME* **119** 354
[12] Ma Q and Clarke D R 1995 *J. Mater. Res.* **10** 853
[13] Stolken J S and Evans A G 1998 *Acta Mater.* **46** 5109
[14] Lam D C C, Yang F, Chong A C M, Wang J and Tong P 2003 *J. Mech. Phys. Solid* **51** 1477
[15] McFarland A W and Colton J S 2005 *J. Micromech. Microeng.* **15** 1060
[16] Kong S, Zhou S, Nie Z and Wang K 2008 *Int. J. Eng. Sci.* **46** 427
[17] Maranganti R and Sharma P 2007 *J. Mech. Phys. Solids* **55** 1823
[18] Park S K and Gao X L 2006 *J. Micromech. Microeng.* **16** 2355
[19] Yang F, Chong A C M, Lam D C C and Tong P 2002 *Int. J. Solids Struct.* **39** 2731
[20] Wang L 2010 *Fluids and Structures* **26** 675
[21] Xia W and Wang L 2010 *Microfluidics and Nanofluidics* **9** 955
[22] Wang L, Liu H T, Ni Q and Wu Y 2013 *Int. J. Eng. Sci.* **71** 92
[23] Kahrobaiyan M H, Khajehpour M and Ahmadian M T *ASME Conf. P.*, November 11–17, 2011, USA
[24] Suga K, Takenaka S, Ito T and Kaneda M 2010 *Adv. Appl. Math. Mech.* **2** 609
[25] Swift M R, Orlandini E, Osborn W R and Yeomans J M 1996 *Phys. Rev. E* **54** 5041
[26] Hu G H, Zhou Z W and Shi Z Y 2010 *Acta Phys. Sin.* **59** 2595 (in Chinese)
[27] Soe M, Vahala G, Pavlo P, Vahala L and Chen H 1998 *Phys. Rev. E* **57** 4227
[28] Zheng L, Shi B C and Chai Z H 2006 *Chin. Phys.* **15** 1855
[29] Peng Y, Shu C and Chew Y T 2003 *Phys. Rev. E* **68** 026701
[30] Ran Z 2009 *Chin. Phys. B* **18** 2159
[31] Li H B and Lü X Y 2001 *Acta Phys. Sin.* **50** 422 (in Chinese)
[32] Ladd A 1994 *J. Fluid Mech.* **271** 285
[33] Ladd A 1994 *J. Fluid Mech.* **271** 311
[34] Krafczyk M, Tolke J, Rank E and Schulz M 2001 *Comput. Struct.* **79** 2031
[35] Kwon Y W 2006 *Eng. Comput.* **23** 860
[36] Kollmannsberger S, Geller S, Düster A, Tölke J, Sorger C, Krafczyk M and Rank E 2009 *Int. J. Numer. Meth. Eng.* **79** 817
[37] Li W, Wei X and Kaufman A 2003 *Vis. Comput.* **19** 444
[38] Kuznik F, Obrecht C, Rusaouen G and Roux J J 2010 *Comput. Math. Appl.* **59** 2380
[39] Frisch U, Hasslacher B and Pomeau Y 1986 *Phys. Rev. Lett.* **56** 1505
[40] Bhatnagar P L, Gross E P and Krook M K 1954 *Phys. Rev.* **94** 511
[41] Bungartz H J, Mehl M and Schäfer M 2010 *Fluid Structure Interaction II: Modelling, Simulation, Optimization* (Berlin/Heidelberg: Springer-Verlag) p. 299
[42] Guo Z L, Zheng C G and Shi B C 2002 *Chin. Phys.* **11** 366